ABSTRACT

ELASTIC SCATTERING AND REACTIONS

IN THE BOMBARDMENT OF ^{14}N

BY 20 MeV DEUTERONS

by William Lucas Pickles

Reported in this thesis are differential cross sections from 10 to 170 degrees, and total cross sections for the following reactions at 20.13 MeV:

$^{14}N(d,d)^{14}N$	
$^{14}N(d,d')^{14}N^*$	EX < 14 MeV
$^{14}N(d,t)^{13}N$	EX < 8 MeV
$^{14}N(d,^3He)^{13}C$	EX < 8 MeV
$^{14}N(d,^4He)^{12}C$	EX < 13 MeV

And total reaction cross sections for the following:

$^{14}N(d,pN)$	E > 2.5 MeV
$^{14}N(d,p)$	Ex < 10 MeV
$^{14}N(d,^4He\ X)Y$	E > 2.5 MeV

The total reaction cross section for deuterons or ^{14}N is computed considering all of the above.

Also reported are differential cross sections from 15 to 50 degrees and total cross sections for the following:

$^{16}O(d,d)$
$^{16}O(d,d')^{16}O^*$ EX < 14 MeV
$^{16}O(d,^4He)^{14}N$ EX < 13 MeV

The elastic cross section $^{14}N(d,d)$, has absolute errors of less than two per cent. Optical potentials have been fit to this data using Snoopy Two. Many essentially equivalent potentials have been found. The potential with the lowest CHI-SQUARED per point (34.5) has a volume imaginary term (W_s) of 3.62 MeV and a surface imaginary term (W_D) of 2.36 MeV, with the imaginary radius parameter 1.63 fermis. Most deuteron potentials found in the literature have W_s equal to zero.

A best optical potential with $W_s = 0$ and one with $W_s = 3.62$ have been used to repeat a DWBA calculation of the cross section for $O^{16}(p,d)^{15}N$ without a major difference in the result. The Isotopic spin for many levels of ^{14}N up to 14 MeV have been assigned as zero on the basis of the $^{14}N(d,d')^{14}N^*$ measurements. The angular distributions and total cross sections in the $^{14}N(d,d')^{14}N^*$ reaction are discussed in terms of weak coupling between two 1^+ nucleons and the 2^+ and the 3^- configuration ^{12}C and between two 1^+ holes and the 3^- configuration of ^{16}O.

Experimentally, gas targets and their use in absolute cross section measurements is discussed. Time-of-flight was used to identify reaction products and is compared to the $E\Delta E$ method of particle identification.

Automatic computer data processing was used extensively and is also discussed. A complete prescription for the fabrication of 3 mm silicon surface barrier detectors is presented and there is a discussion of the use of various types of detectors in time-of-flight work.

ELASTIC SCATTERING AND REACTIONS IN THE BOMBARDMENT OF ^{14}N BY 20 MeV DEUTERONS

by

William Lucas Pickles

A THESIS

Submitted to

Michigan State University

in partial fulfillment of the requirements

for the degree of

DOCTOR OF PHILOSOPHY

Department of Physics

1970

ACKNOWLEDGMENTS

I want to express my appreciation of the excellent educational environment offered by the Michigan State University Cyclotron Laboratory. All of the faculty, staff, and students have been fully involved in guidance and assistance before and throughout the work presented in this thesis. I also deeply appreciate the complete access I have had to all the facilities of the laboratory.

I have tried to include the specific acknowledgments of most of the contributions to this work by people in our laboratory in the section which involves their contribution. However, let me take this opportunity to thank L. L. Learn, Prof. E. Kashy, Dr. G. F. Trentelman, and I. D. Proctor, who worked many hours to help me collect the data presented here, and D. S. Sosnoski and J. C. Pickles, who were of invaluable assistance during the data reduction and preparation of the manuscript. I am indebted to Mrs. M. E. Krueger for her excellent cooperation in the typing of this thesis.

Prof. E. Kashy has performed the extremely important function of suggesting the dimensions of this work so that they included as much of the educational benefits in our laboratory as possible.

I would also like to express my deep appreciation for the patience and support of my wife, Judy.

TABLE OF CONTENTS

LIST OF TABLES

LIST OF FIGURES

1. INTRODUCTION

The work presented in this thesis consists principally of the accurate measurement of the differential cross sections for elastic and inelastic scattering of 20 MeV deuterons from ^{14}N. The results are analyzed to obtain optical model parameters for $^{14}N(d,d)$ and spectroscopic information about the T = 0 states of ^{14}N.

The choice of ^{14}N resulted from a continuing interest in light nuclei at this laboratory and the energy was chosen as the minimum deuteron exit energy for which consistent spectroscopic information from the (p,d) reaction on light elements were obtained (Sn 69). Accurate proton and deuteron optical potentials are desirable in the DWBA analysis of the (p,d) reaction, because the effects of the distortion of the exit channel wave-functions have strong effects upon the calculated reaction differential cross sections.

Good proton optical potentials for energies below 50 MeV are available in the literature. Deuteron optical potentials in the energy region of 20-50 MeV are available (Mc 69, Hi 68), but the data from which they are extracted are in general less complete and less accurate than the corresponding proton data. For example, deuteron elastic scattering and/or fits at angles greater than 100 degrees

center-of-mass are rare in this energy region. The elastic deuteron cross sections presented in the work have absolute errors of less than 2% and extend in the laboratory frame from 10 degrees to 170 degrees. This data has been fit using the optical code "SNOOPY TWO" (Sc 69). Several sets of acceptable optical potentials have been found, the quality of the fit, however, especially for angles greater than 100°, is not as good as that usually obtained for proton elastic scattering. The elastic cross section and optical fits are discussed in detail in Sec. 4.1 and 4.2.

The DWBA calculations for $^{16}O(p,d)^{15}O^*$ (Ex = 6.180 MeV) performed by Snelgrove (Sn 69) have been repeated using the $^{14}N(d,d)$ parameters from this work. Peak to valley ratio of the calculated deuteron cross-section oscillations is in close agreement with Snelgrove's experimental data, but the new deuteron optical potentials do not change the calculated back angle (p,d) cross section. The conclusion is that lack of agreement between Snelgrove's DWBA calculations and his back angle data was not due to inaccurate deuteron optical potentials, but more likely, resides in the form factor for the reaction as was previously suggested (Sn 69, Pr 70).

The deuteron is a particle whose isospin is zero, consequently in the (d,d') reaction only states with isospin equal to that of the ground-state should be excited.

This selection rule removes from the observed spectrum of $^{14}N(d,d')^{14}N^*$ approximately one-third of the known states below 13 MeV. This fact alone makes the (d,d') data interesting. It means that most T = 0 states in ^{14}N are well resolved in a counter experiment whose energy resolution is 45 to 70 KeV. No evidence for the excitation T = 1 states in the $^{14}N(d,d')$ reaction have been found and upper limits of cross-sections for breaking of the T = 0 selection rule for several of these states have been set. This matter is discussed in Sec. 5.1.

The spectroscopic information about ^{14}N presented in this work is derived from total reaction cross-sections and angular distributions for $^{14}N(d,d')^{14}N^*$, $^{16}O(d,d')^{16}O^*$, and $^{16}O(d,^4He)^{14}N^*$ and from DWBA analysis of the $^{14}N(d,d')^{14}N^*$.

Measurement of cross-sections with absolute error less than 2% represents a considerable experimental effort and the successful use of time-of-flight for particle identification in taking spectra represents a departure from the standard experimental procedures used in our laboratory. Consequently, Sec. 2 contains an extensive discussion of errors, experimental systems, and time-of-flight techniques.

Differential cross-sections and total reaction cross-section for the $^{14}N(d,t)$, $^{14}N(d,^3He)$, $^{14}N(d,^4HeX)Y$, $^{14}N(d,pn)Y$, and $^{14}N(d,p)$ were measured simultaneously with

the reactions previously discussed and have been used principally to construct an "anatomy" of deuteron scattering. The possible implications for deuteron optical potentials from the fact that 60% of total reaction cross-section comes from the one channel $^{14}N(d,pn)Y$ are discussed in Sec. 5.3.

2. EXPERIMENTAL

2.1 Experimental-General Discussion

The measurement of differential cross sections with small absolute errors was the primary goal of the experimental systems. The procedures are described in this section.

The following expression for differential cross section is a result of considering $\frac{d\sigma}{d\Omega}$ to be the area per nucleus which causes a particular type of scattering into unit solid angle at an angle θ with respect to the beam.

$$\frac{d\sigma(\theta)}{d\Omega} \equiv \underset{SA\to 0}{\text{Limit}} \frac{N_p}{N_T N_B SA} \frac{cm^2}{sr.} \qquad (2.1)$$

N_p is the number of particles scattered from a target of N_T nuclei per cm^2. N_B is the total number of incident beam particles and SA is the solid angle defined by the slit in front of the detector. Re-expressing the above equation yields

$$\frac{d\sigma(\theta)}{d\Omega} \equiv \underset{\substack{A\to 0 \\ R\to R}}{\text{Limit}} \frac{N_p}{(\bar{\rho}t)(Q/e)A/4\pi R^2} \frac{cm^2}{sr.} \qquad (2.2)$$

where Q is the total charge of the beam which is incident on the target; e is the charge per beam particle. A is

the area at the detector through which a particle must pass in its free flight from the target to the detector. All defining slits have some thickness but may not in fact stop all scattered particles incident on them. Consequently, these particles may be small-angle-scattered from the surface of the hole through the defining slit. The particle undergoing rescattering of this type may enter the detector and will be kinematically down shifted in energy and/or degraded by energy loss to the slit. In summary, any absorber with a hole of area A cut through it will have an area ΔA surrounding the hole which has an opacity different from either the hole (0 opacity) or the absorber. Fortunately particles that pass through ΔA traveling from the target to the detector have a lower energy than the particles which reach the detector surface without interacting with the absorber. "Slit scattering" is the primary example of this effect. Slit scattered counts must be subtracted from N_p. A, then, is the number which is to be interpretated as the area of the clear hole in a defining absorber placed near the front surface of the detector. In expression 2.1 t is the length parallel to the incident beam in which target nuclei exist which may cause scattering into the detector. $\bar{\rho}$ is the average number density per cm^2 of target nuclei in the region t. $\bar{R}$ is the average distance from region t to the center of the defining absorber or slit at the detector.

We can now discuss the problems encountered in measuring $\bar{\rho}$ and Q. $\bar{\rho}$ must be known and remain constant during an experiment or be measured as $\frac{d\sigma}{d\Omega}$ is being measured. Usually a monitor counter serves to measure the product $\frac{\bar{\rho}tQ}{e}$ during the measurement of $\frac{d\sigma}{d\Omega}$. Solid targets melt, evaporate, pick up oil from the vacuum system and in general must be monitored during an experiment. In addition a separate experiment must be performed on the target to measure the initial $\bar{\rho}$. Errors are generated at each step. A gas target requires only that you measure the pressure and temperature of the gas contained to determine $\bar{\rho}$. For this reason gas targets were used in this experiment and are discussed in detail in Sec. 2.4.

Q is the charge of the beam incident on the target. Since the total number of particles scattered out of the beam is small, Q can be taken as the beam charge collected by stopping the beam after it has passed through the target. There are several ways errors can be committed in collecting Q. The beam is diverging when it leaves the target due to small angle scattering and you must be sure to "catch" all of it. When the beam is stopped by the material in the faraday there is a copious emission of electrons. These electrons must not escape from the collecting part of the cup. The target is also an electron emitter when beam is passing through it and these target electrons must be kept

out of the collecting cup. Having made sure the charge on the cup is due only to the beam and none of it has been lost, it must then be integrated accurately without losses. All of these considerations are discussed in Sec. 2.5.

N_p, the number of scattered particles passing "freely" through A, will, except for an error in background estimation, be too small. That is, you may miss counts, but it is highly unlikely you will make extra ones. The detector itself may fail to give the event its correct pulse height for several reasons:

1. Excitation of detector (Si) nuclei
2. Charge collection failure
3. Reactions in the detector such as (d,pn)
4. Pileup (Two scattered particles arriving within the collection time of the detector)

The electronic recording system has a processing time per event during which it will not process another event. A typical time for processing was 40 μs. This effect is called dead time and was measured using pulses from the monitor counter.

The particle identification system may fail for a number of reasons, and lose an event. In particular, when time-of-flight is used the time signal may not be generated, leaving only an energy signal. In this

experiment, events without a time signal were recorded in order to measure this type of loss.

All of the losses described above were measured during this experiment and are discussed in Secs. 2.6 and 2.7.

The ^{14}N data presented in this thesis was taken in 96 hours of continuous running and the ^{16}O in 48 hours. Particle identification was achieved with time-of-flight techniques and a 2-dimensional data taking routine "TOOTSIE" written for the XDS Sigma-7 computer by D. L. Bayer of this laboratory (Ba 69).

2.2 Beam and Beam transport

The 20 MeV beam of deuterons used in this experiment was produced by the MSU Cyclotron. Figure 2.1 shows a general view of the cyclotron and transport system. The beam extracted was normally 1 to 5 μ amps with a time resolution of less than 0.4 ns. This narrow time width was achieved in most cases by using internal phase slits, or occasionally only the beam transport system slits. Time resolution was never worse than 0.5 ns.

The beam analysis system is basically an object slit (Box 3), a 90° bending and dispersion system, and an energy defining slit (Box 5), with appropriate quadrupole and sextupole focusing (Ma 67). Also used in this experiment

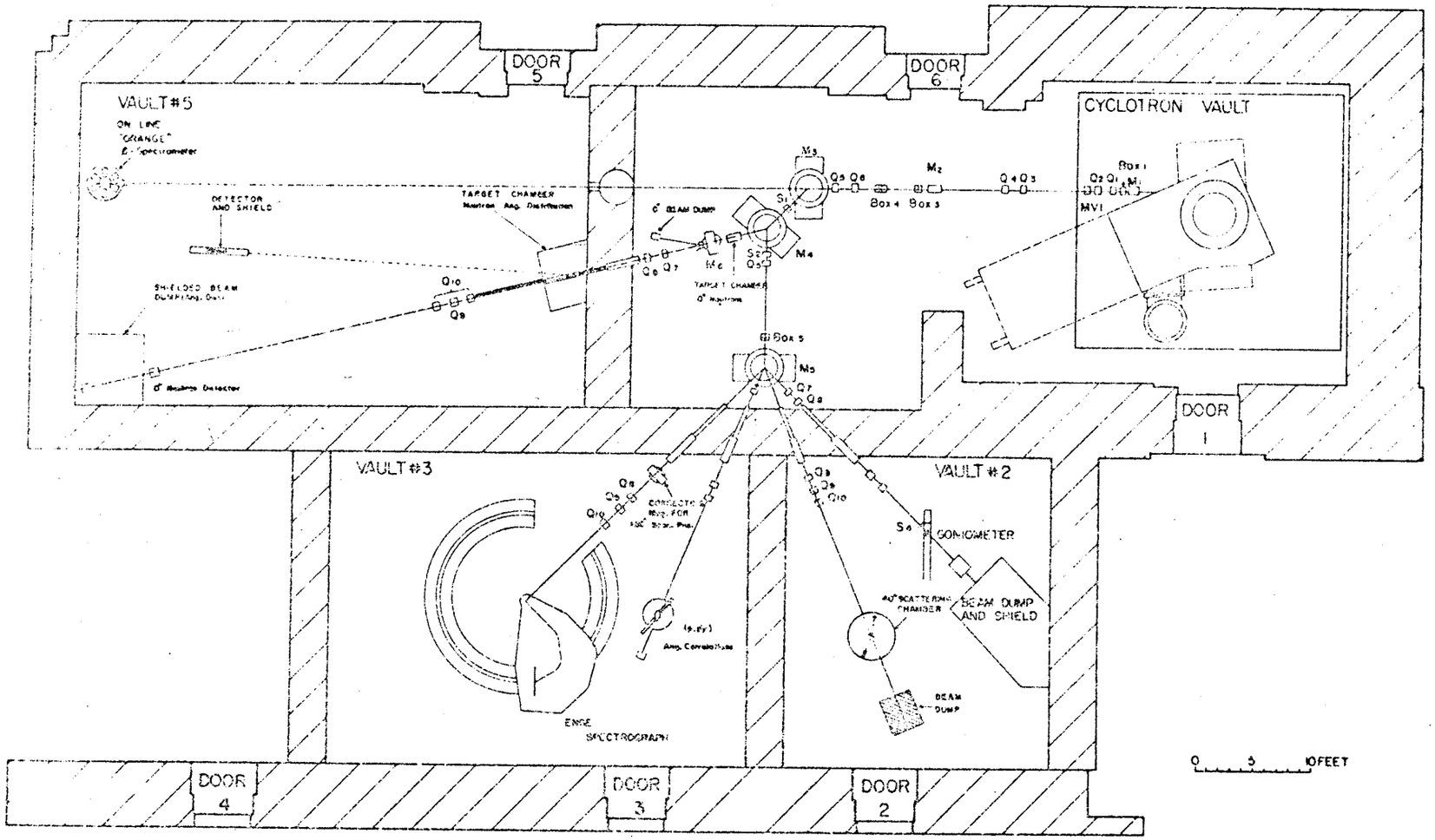

Figure 2.11 Layout of Cyclotron experimental areas as of August 1970. The new neutron angular distribution facility which is being designed will have a fixed flight path extending to the left from "Box 5" and a moveable magnet to bring the beam into Box 5 from any angle.

was a set of slits (Box 10) located immediately after the last quadrupole, a set of defining slits (Box 11) at the entrance to the scattering chamber, and magnetic steering at Box 10. All exposed beam pipe was shielded from stray magnetic fields with soft iron. The Box 10 and 11 slits and Box 10 steering magnet were used to define the zero angle for scattering and insure that it remained constant during the taking of data (Sec. 2.32).

The beam was focused at the center of the scattering chamber with a magnification of.8 of the Box 5 object. Typically the beam spot size was 0.070 inches horizontally and vertically. A maximum of 400 na was delivered to the scattering chamber; typical currents were 80 and 100 na.

2.3 Scattering Chamber and Scattering Angle Measurement

2.31 General

Figure 2.31 shows a schematic of the experimental area. Included are the last focusing elements in the beam line, the scattering chamber, and the aparatus used to define the zero scattering angle. The chamber itself was 30 inches in diameter, had one remotely moveable counter arm and one fixed arm. The detector and collimating units for counting the scattered particles were mounted on the moveable arm. The monitor counter and its collimating unit were mounted on the fixed arm. The gas cell targets and scintallator were mounted on a 1/4 inch dowel that defined the center of rotation of the moveable arm. The targets rotation and height could be controlled from the data room. A typical pressure obtained in the chamber was 10^{-5} torr.

The scattering chamber was equipped with an electrical angular readout, but this was found to reproduce measurement to only 0.2 degrees. An angular readout system which was accurate to better than 0.1 degrees and did not require constant checking was necessary. The system devised included a protractor and vernier which was read through a magnifying optical system by closed circuit T. V.

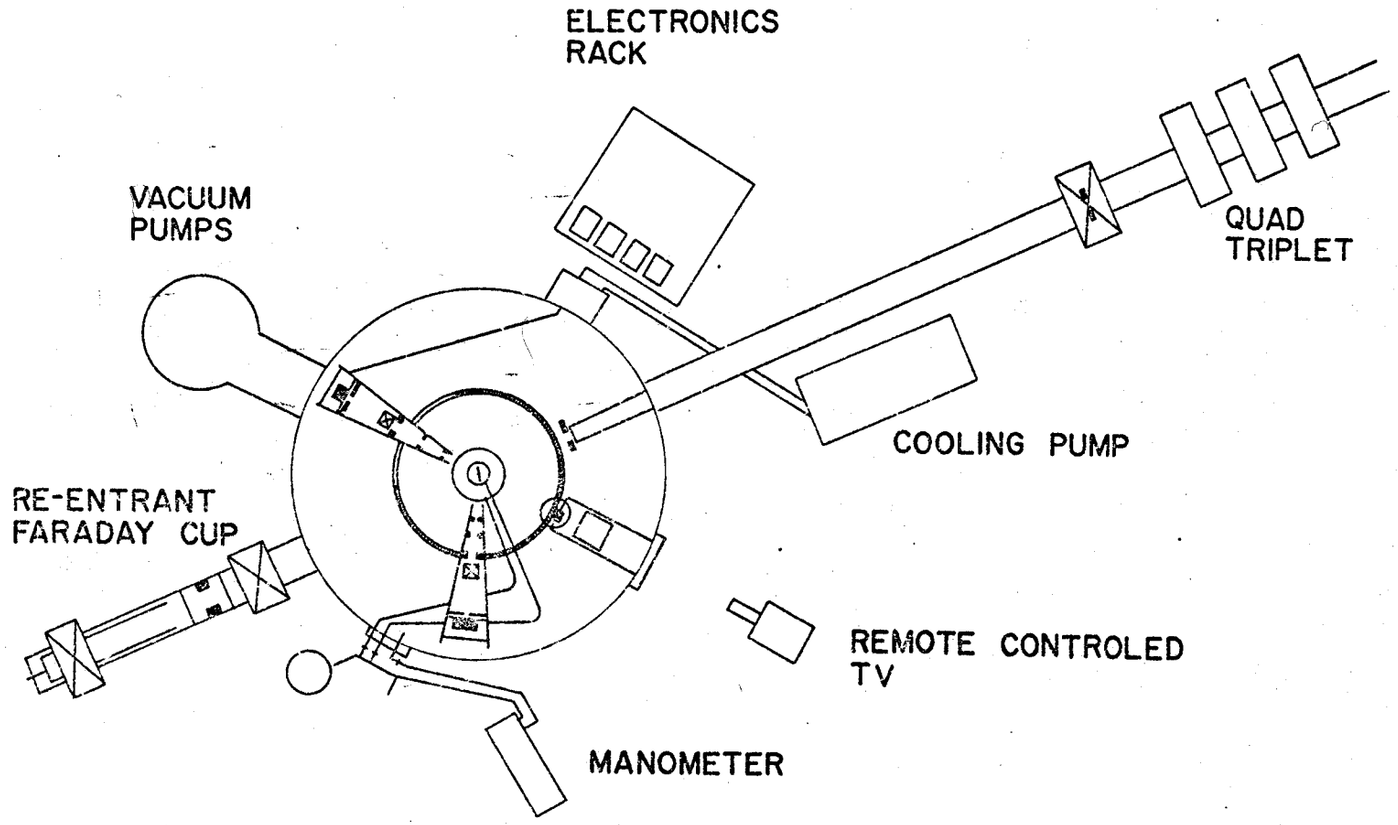

Figure 2.31 Schematic of
Experimental Area.

2.32 Angle Measurement and Errors

Figure 2.32 shows in two views, the center of the scattering chamber and the apparatus constructed to measure the angle of the moveable scattering arm with respect to the beam. An aluminum protractor 15±.001 inches in diameter and 1/4 inch thick was machined in our shop by N. R. Mercer. The angular scribe marks were cut using a dividing head with a maximum angular error of 0.015 degrees; calculated as follows:

$$\Delta\theta = 57 \times \frac{(\text{center error} + \text{scribe error})\{\text{inches}\}}{\text{Radius}\{\text{inches}\}} \quad (2.3)$$

In this case:

$$\Delta\theta = \frac{5.7 \times 2 \times 10^{-3}}{7.5} \approx 0.015 \text{ degrees}$$

A vernier was also machined to the same accuracy. The scribe marks on the protractor were cut every 0.2 degrees. This protractor was then bolted to the rotating scattering arm. The vernier was mounted on a support which was bolted to the viewing port wall. The vernier was adjustable in all directions. This whole assembly was quite massive and very stable when finally installed. The protractor was then adjusted so that its center was the actual center of rotation of the scattering arm. This was accomplished by adjusting the position of the protractor and the vernier until an equal

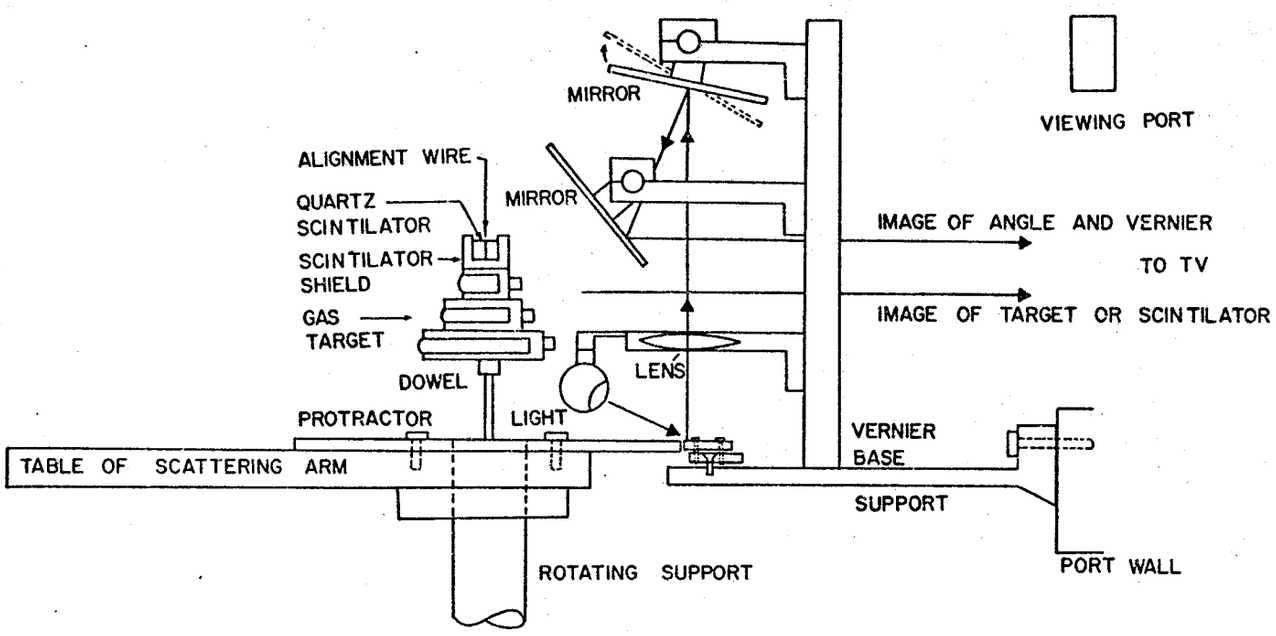

SIDE VIEW OF PROTRACTOR VERNIER AND MOUNT MIRRORS GAS TARGETS WITH SCINTILATOR AND ALIGNMENT WIRE AND SCATTERING TABLE

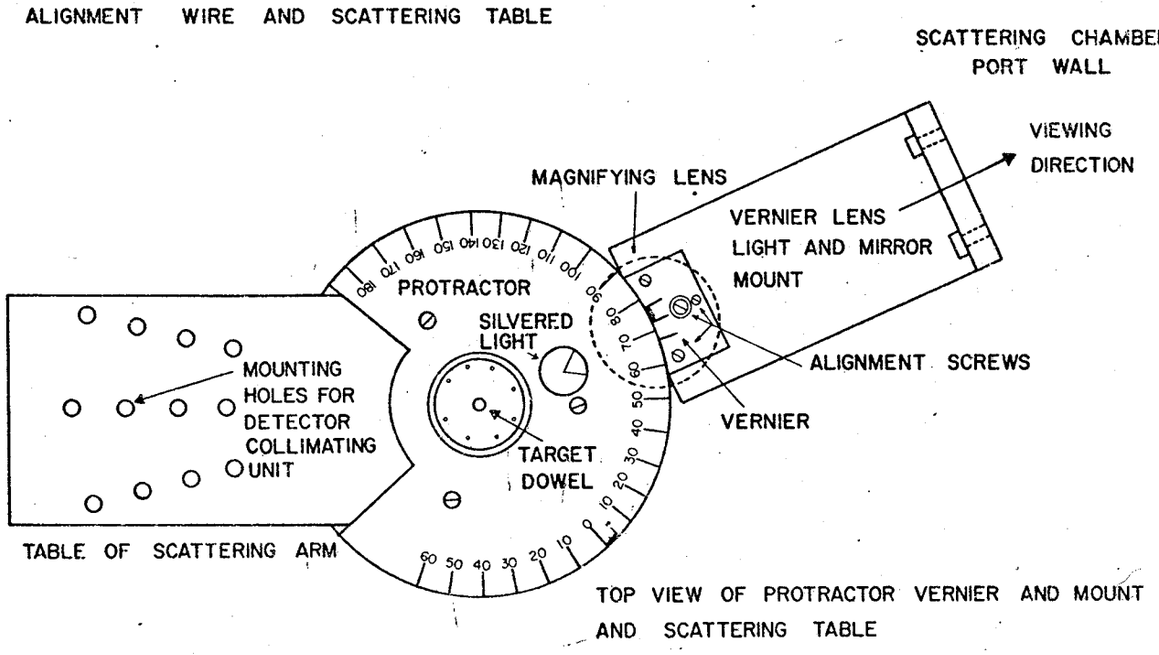

TOP VIEW OF PROTRACTOR VERNIER AND MOUNT AND SCATTERING TABLE

Figure 2.32 PROTRACTOR VERNIER AND OPTICAL READOUT FOR SCATTER ANGLE MEASUREMENT

distance was maintained between the edge of the protractor and the edge of the vernier for the full rotation of the protractor. The estimated centering error was 0.001 inches. Adding these errors linearly, the basic angular error of the protractor-vernier combination was approximately 0.025 degrees. The vernier marks were constructed to allow reading of angles to 0.02 degrees.

As is shown in Figure 2.32 a silvered bulb illuminated the vernier and protractor scale which was then viewed through a magnifying lens and two mirrors by a T. V. camera with a150 mm telephoto lens. This camera had a remote focus and orientation control. Two mirrors were employed to produce a non-inverted image. The T. V. camera also provided a clear view of the target area with only a small adjustment of the camera.

The total relative angular error was 0.1 degrees and is due to the error in alignment of collimating units, the fact that there was an uncertainty of 0.020 inches in placing the beam relative to the center of rotation, and on error in determining 0 degrees. A centering error will produce an angular error $\Delta\theta$ which goes as:

$$\Delta\theta = 57 \times \frac{\Delta C}{R} \times \cos\Phi \text{ degrees} \qquad (2.32)$$

Where R is radius at which the angle θ is measured, ΔC is the centering error and Φ is the angle between the direction

of the maximum centering error and the direction at which the angle measurements were made. The collimating units for the detector had two slits 10 inches apart with rear slit 15 inches from the center of rotation of the scattering arm. Using a surveying telescope it was determined that the center of observation looking through the two slits was 0.005 inches off the center of rotation. Thus $\Delta\theta$ is equal to 0.020 degrees.

$$\Delta\theta = 57 \times \frac{5}{15} \times 10^{-3} \simeq 0.020 \text{ degrees}$$

The beam spot was typically 0.060 inches in diameter, and an error of 0.020 inches for the centroid of the beam was estimated. This results in a relative-angle uncertainty of 0.082 degrees, and it the principal source of angular error.

$$57 \times \frac{20}{14} \times 10^{-3} \simeq 0.082 \text{ degrees}$$

Combining the 3 sources of relative-angle error linearly yields a maximum error of 0.127 degrees.

$$0.082 + 0.020 + 0.025 \simeq 0.127 \text{ degrees}$$

Adding in quadrature, the error is 0.09 degrees.

2.33 Zero Angle Determination and Error

The beam direction and centering was fixed by insuring that the beam traveled in a straight line between two widely spaced slits, and passed over the center of rotation of the scattering arm.

Figure 2.33 shows these slits at boxes 10 and 11. Magnetic shielding was wrapped around the beam pipe between these two sets of slits. A small electromagnet M10 was located next to the Box 10 slit towards the cyclotron (up-stream from Box 10). Box 11 was located inside the scattering chamber 10 inches from the center and consisted of two vertical and two horizontal tantalum slits 0.125 inches thick. Charge could be collected from all four independently. Box 10 consisted of two horizontal plane slits made of aluminum with tantalum edges. The Box 10 slits were remotely moveable, while the Box 11 slits were fixed during the line up procedure.

The alignment of Box 10 and Box 11 slits was accomplished as follows: A surveying telescope was sighted through the faraday cup port, over the raised center dowel in the scattering chamber, through the Box 11 slits, through the Box 10 slits and focused on a pin at the center of the steering magnet M5. This pin and a reference surveyors target on the wall behind the telescope were used to establish the height of the beam (the optical center vertically of

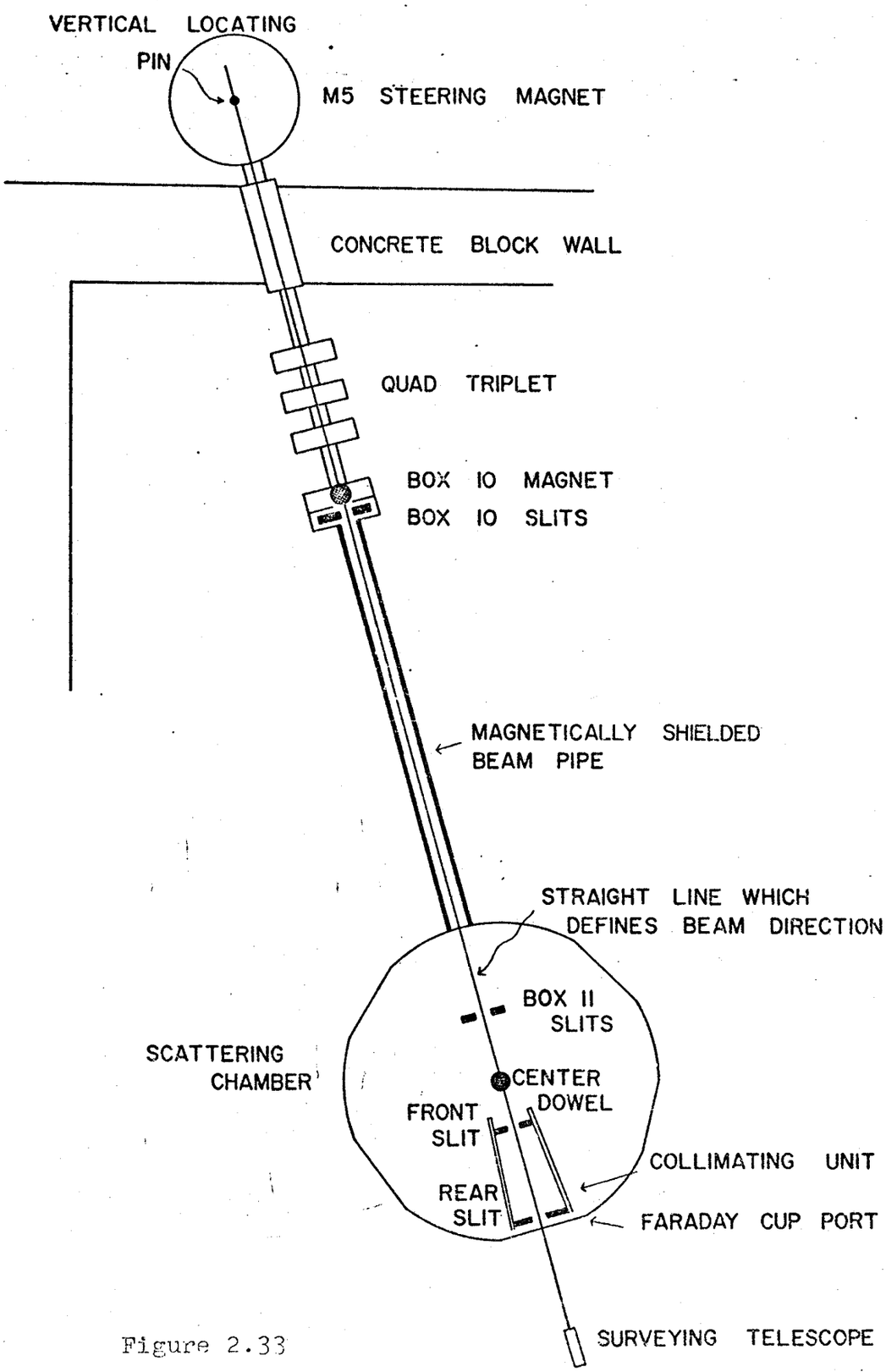

Figure 2.33

BEAM LOCATION SYSTEM